CHEMMEDCHEM

CHEMISTRY ENABLING DRUG DISCOVERY

Accepted Article

Title: Computer-assisted selective optimization of side-activities - from cinalukast to a PPARα modulator

Authors: Julius Pollinger, Simone Schierle, Sebastian Neumann, Julia Ohrndorf, Astrid Kaiser, and Daniel Merk

To be cited as: *ChemMedChem* 10.1002/cmdc.201900286

Link to VoR: http://dx.doi.org/10.1002/cmdc.201900286

A Journal of

ChemPubSoc Europe

WILEY-VCH

www.chemmedchem.org

10.1002/cmdc.201900286

WILEY-VCH

FULL PAPER

Computer-assisted selective optimization of side-activities - from cinalukast to a PPARα modulator

Julius Pollinger[a]#, Simone Schierle[a]#, Sebastian Neumann[a], Julia Ohrndorf[a], Astrid Kaiser[a], and Daniel Merk*[a]

[a] Julius Pollinger, Simone Schierle, Sebastian Neumann, Julia Ohrndorf, Astrid Kaiser and Dr. Daniel Merk (ORCID: 0000-0002-5359-8128)
Institute of Pharmaceutical Chemistry
Goethe University Frankfurt
Max-von-Laue-Str. 9, D-60438 Frankfurt, Germany
E-mail: merk@pharmchem.uni-frankfurt.de
# Julius Pollinger and Simone Schierle contributed equally to this work and are listed in alphabetical order

Supporting information for this article is given via a link at the end of the document.

Abstract: Automated computational analogue design and scoring can speed up hit-to-lead optimization and appears particularly promising in selective optimization of side-activities (SOSA) where possible analogue diversity is confined. Probing this concept, we employed the cysteinyl leukotriene receptor 1 ($CysLT_1R$) antagonist cinalukast as lead for which we discovered peroxisome proliferator-activated receptor α (PPARα) modulatory activity. We automatically generated a virtual library of close analogues and classified these approx. 8000 compounds for PPARα agonism and $CysLT_1R$ antagonism using automated affinity scoring and machine learning. A computationally preferred analogue for SOSA was synthesized and in vitro characterization indeed revealed a marked activity shift towards enhanced PPARα activation and diminished $CysLT_1R$ antagonism. Thereby, this prospective application study highlights the potential of automating SOSA.

Introduction

Computer-assisted drug discovery increasingly strives to automate structural optimization of bioactive small molecules in order to minimize experimental efforts.[1] Repeated design-synthesize-test cycles of typical hit-to-lead expansion in medicinal chemistry may considerably profit from modern computational approaches to compound prioritization. A particular promising application of such virtual compound optimization lies in its combination with the concept of selective optimization of side-activities[2,3] (SOSA) where (weak) off-target activities of approved or experimental drugs are turned into the main activity of a new, closely related structural analogue while diminishing the activity on the original target. A great advantage of this concept are the superior properties of drugs being used as lead compounds. Since drugs have already been optimized for favorable physicochemical properties, bioavailability and safety, the starting point of SOSA-based drug discovery is by definition drug-like. However, in order to conserve the favorable drug-like properties of the lead compound selected for a SOSA campaign, structural modifications usually need to be kept small during optimization. Within such confined chemical space, virtual prioritization of a drug's structural analogues for predicted activity on the desired side-target appears very promising.

To probe this concept of computer-assisted SOSA, we have selected the cysteinyl leukotriene receptor 1 ($CysLT_1R$) antagonist cinalukast (**1**) as lead compound for which we have discovered weak partial agonistic activity on peroxisome proliferator-activated receptor α (PPARα)[4,5] in a systematic screening campaign. The fatty acid mimetic[6] cinalukast (**1**)[7,8] has favorable physicochemical properties and its modular architecture allows various structural modifications. Thus, **1** appears well suitable for SOSA but its low-yielding 5-step synthesis renders a systematic structure activity relationship (SAR) study of **1** an elaborate task. We employed **1** as lead for computer-assisted SOSA aiming to structurally optimize the drug's PPARα agonism. We automated the design of cinalukast analogues and their activity prediction on PPARα and $CysLT_1R$. After successful proof-of-concept evaluations, a computationally preferred analogue was synthesized and biologically characterized. It comprised higher activity on PPARα than **1** and simultaneously revealed markedly reduced $CysLT_1R$ antagonism confirming the potential of this computer-assisted structural optimization approach.

Results and Discussion

Synthesis

Cinalukast derivatives **2**-**4** were synthesized in five to six steps according to Scheme 1 starting from bromomethylketones **5**-**6** which were first cyclized with thioacetamide (**7**) to 2-methylthiazoles **8** and **9**. 4-*tert*-Butyl-2-methylthiazole **10** was commercially available. Condensation of **8**-**10** with 3-nitrobenzaldehyde (**11**) to nitrostyrylthiazoles **12**-**14** followed by reduction with $SnCl_2$/HCl then produced aminostyrylthiazoles **15**-**17**. Further reduction of the styryl moiety in **15** with H_2/Pd(C) afforded phenethylthiazole **18**. **16**-**18** were then coupled with dicarboxylic acid monoethylesters **19** and **20** to obtain esters **21**-**23** using EDC*HCl and 4-DMAP, and saponification of **21**-**23** yielded test compounds **2**-**4**. *E/Z*-isomerism was observed for **2**

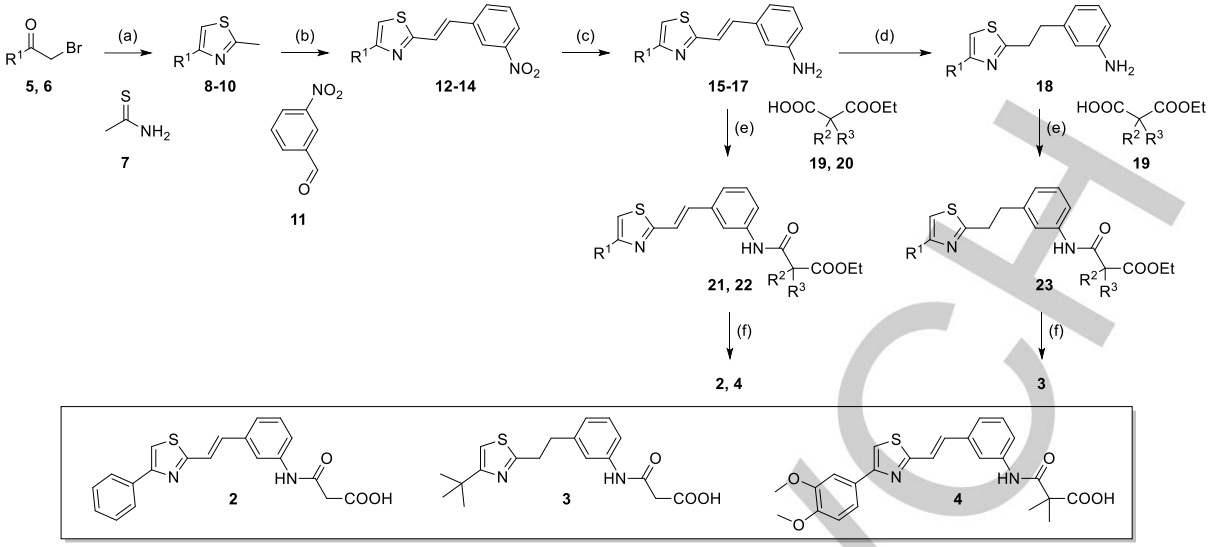

Scheme 1. Synthesis of cinalukast derivatives **2**-**4**. Reagents and conditions: (a) thioacetamide, DMF, reflux, 4 h, 74-82%; (b) NaOAc, HOAc, reflux, 10 h, 14-24%; (c) $SnCl_2$, EtOH, 65°C, 2-3 h, 55-66%; (d) H_2 (1 bar), Pd(C), rt, 18 h, 94%. (e) EDC*HCl, 4-DMAP, $CHCl_3$, 60°C, 12-16 h, 14-28%; (f) LiOH, THF/H_2O, rt, 12 h, 21-71%.

and **4** and their *E*-isomers (*E/Z* > 95%) were isolated for in vitro pharmacological characterization by preparative HPLC. The commercial sample of **1** contained the pure *E*-isomer. The observed *E/Z*-isomerism turned out to be light dependent but was not observed under the conditions of the in vitro test system used in this study confirming that it does not affect the activity data (see Supporting Information for details).

Biological evaluation

PPARα modulatory activity of **1** and derivatives **2**-**4** was determined in a specific PPARα-Gal4-hybrid reporter gene assay[9,10] relying on a chimeric receptor composed of the human PPARα ligand binding domain (LBD) and the DNA binding domain of the receptor Gal4 from yeast to govern reporter gene expression. A Gal4-inducible firefly luciferase served as reporter and a constitutively expressed renilla luciferase was used to monitor test compound toxicity and transfection efficiency. $CysLT_1R$ antagonism of **1** and **4** was assessed in a cell-based Ca^{2+}-flux assay in competition with 0.1 nM leukotriene D4[11].

Computer-assisted structural optimization

Characterization of cinalukast (**1**) on therapeutically relevant nuclear receptors revealed partial agonistic activity on PPARα (EC_{50} = 10±2 µM, 5.3±0.6-fold activation). With this attractive side-activity, **1** was chosen as lead for SOSA-based optimization towards PPARα agonism with computational support. To predict the potency of **1** and analogues on the nuclear receptor PPARα, we have chosen the HYDE scoring function[12]. HYDE estimates free energies of binding for ligand-protein complexes focusing on hydrogen bond formation between ligand and protein as well as dehydration of binding sites[12]. Therein, it considers ligand geometry and interaction angles. HYDE was successfully applied on hydrophobic ligand binding sites previously[13–16] and appeared suitable for predicting the interaction of **1** and analogues with the highly lipophilic PPARα ligand binding site. Although scoring functions for computational ranking of protein-ligand interactions in many cases are error-prone, it was shown that scoring can have predictive power and provide reliable correlation between computational score and biological potency for some targets[17,18]. Especially for PPARs[18] scoring may be applied successfully when the co-crystallized ligand in the template used for scoring sufficiently resembles the studied molecules.

Aiming to evaluate the suitability of HYDE for our approach, we first studied the correlation between the HYDE score for analogues of **1** concerning affinity to PPARα and their activity on the nuclear receptor. For this proof-of-concept, we selected simple building blocks that were available in house to minimize synthesis efforts and costs. We manually designed a small library comprising 27 derivatives of **1** with variations in the thiazole substituent, in the acidic side chain as well as in the geometry and saturation degree of the central styrylthiazole moiety (Table S1). To prioritize compounds for synthesis, we docked all 27 cinalukast analogues into the PPARα ligand binding site using FlexX[19] and calculated the HYDE scores for the top-ranking poses. The PPARα-LBD complex X-ray 4CI4[20] served as structural template as it contains a ligand with similar linear three-ring structure as **1**. The results suggested that both the thiazole substituent and the acidic side chain length had marked impact on potency (Table S1). Amongst the simplified derivatives with no variations in the central styrylthiazole moiety, compound **2** (Scheme 1) comprising a 4-phenylthiazole moiety and a 3-oxopropanoic acid side chain appeared most favored (-63 kJ/mol).

To computationally assess the importance of the carboxylic acid for HYDE scores on PPARα, we studied the influence of replacing it in **2** with an amide, a nitrile, an alcohol, or a methyl group (Table S2). As expected for the fatty acid sensor PPARα[5], all four replacements were predicted as significantly less active by HYDE. The scores also suggested that a hydrogen bond donor (amide, alcohol) is essential while the scores for the nitrile and the terminal methyl moiety were markedly lower. Based on these observations, we selected carboxylic acid derivative **2** for synthesis and in vitro characterization.

Concerning variations in the styrylthiazole residue, the HYDE results suggested that changes in the geometry would be detrimental (Table S1, row a) for potency on PPARα but that reduction of the styryl residue might be tolerated (Table S1, rows b and c). The 4-*tert*-butylthiazole derivative **3** (Scheme 1) with reduced styryl residue and 3-oxopropanoic acid side chain was

predicted as weak PPARα modulating cinalukast analogue (-55 kJ/mol) and to cover a broader structural variation in this proof-of-concept evaluation, we selected **3** for synthesis and in vitro characterization.

Proof-of-concept cinalukast derivatives **2** and **3** showed partial agonistic activity on PPARα with lower potency and activation efficacy than **1** (**2**: EC_{50} = 11.7±0.5 µM, 3.0±0.1-fold act.; **3**: EC_{50} = 73±17 µM, 3.3±0.5-fold act.; Table S3). No direct correlation between the in vitro potencies of cinalukast (**1**) and derivatives **2** and **3** with their HYDE scores was observed but the prediction agreed well with the rank order of potency, particularly when considering EC_{50} value and activation efficacy. This result sufficiently validated the HYDE-based compound prioritization for further computer-assisted optimization of **1** towards selective PPARα agonism.

As the prospective proof-of-concept study confirmed suitability of HYDE to predict PPARα modulatory potency of **1** and derivatives, we aimed to use this tool in a markedly expanded chemical space of cinalukast analogues considered for structural optimization. For this, we automatically generated a combinatorial library from all suitable building blocks that were commercially available from typical vendors. To retain the basic molecular architecture of drug **1**, consider the observations from the proof-of-concept evaluation, and keep structural changes small according to the SOSA concept, we only varied the thiazole substituent and the acidic side chain. The virtual combinatorial library was generated from bromomethylketones (**A**) for the generation of the 4-substituted styrylthiazole residue as well as haloalkyl carboxylic acid esters (**B**) respectively dicarboxylic acid monoesters (**C**) to introduce the acidic side chain (Scheme 2). The latter (**B**&**C**) covered linear and branched alkyl chains as well as aromatic moieties for broader structural variety. The resulting library contained 7922 cinalukast analogues.

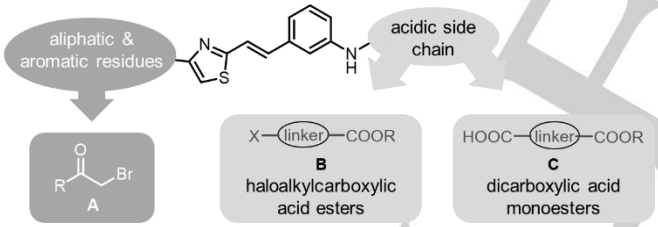

Scheme 2. Virtual combinatorial library design. The thiazole substituent covered aliphatic and aromatic residues with varying size and substitution patterns, the acidic side chain covered aromatic and linear or branched aliphatic carboxylic acid moieties linked to the aminostyryl scaffold via an amine or amide bond.

In an automated workflow, the structures of this virtual combinatorial library were docked with FlexX before the top-scored docking poses were assessed with HYDE for their predicted interaction with PPARα using 4CI4[20] as structural template. According to the SOSA concept, the molecules were also filtered for low lipophilicity (clogP ≤ 4). Among the five computationally favored compounds for interaction with PPARα (Table 1, top-30 in Table S4), the top-3 (**4a**, **4b**, **4**) hardly differed in their scores for PPARα, whereas **4c** and **4d** comprised slightly lower predicted affinities.

Table 1. Computational activity predictions for top-5-ranked entries of the combinatorial cinalukast analogue library. Activity on PPARα predicted by HYDE-based affinity prediction (the respective top-scored pose was considered for each molecule). $CysLT_1R$ antagonism was computationally assessed with a random forest classification model to assign candidates to high (class 1) or low (class 2) $CysLT_1R$ antagonistic potency. Cinalukast (**1**) for comparison. The top-3 compounds **4a**, **4b** and **4** differed marginally in their predicted activities and **4** was selected for synthesis and in vitro characterization based on building block availability.

ID	Structure	**PPARα** HYDE score [a]	**$CysLT_1R$** random forest [b]
1	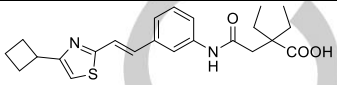	-83	class 1
4a	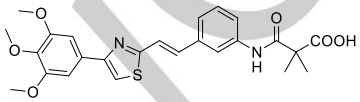	-85	class 2
4b	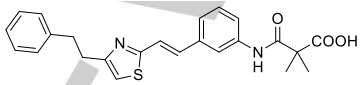	-84	class 2
4	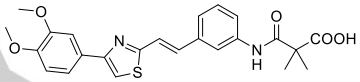	-81	class 2
4c	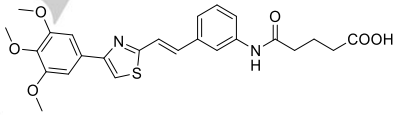	-76	class 2
4d	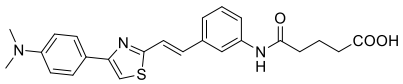	-69	class 2

[a] PPARα affinity prediction (HYDE): kJ/mol. [b] $CysLT_1R$ activity prediction: class 1 - predicted IC_{50} < 1 µM; class 2 - predicted IC_{50} > 1 µM.

We then computationally assessed the potential of these PPARα-favored cinalukast analogues to interact with $CysLT_1R$. Due to the lack of X-ray data of this G-protein coupled receptor as structural template, the computational estimation of $CysLT_1R$ affinity had to follow a ligand-based strategy. We retrieved all available compounds with annotated activity on $CysLT_1R$ from ChEMBL[21] (215 potent antagonists with IC_{50} < 1 µM, 904 weak antagonists with IC_{50} > 1 µM or inactive examples) and used this collection of compounds with reliable activity data to train a random forest model for high/low activity classification on $CysLT_1R$. Known compounds were assigned to two classes with an activity threshold of 1 µM. Molecules were represented by various fingerprints (MACCS[22], Morgan[23], AtomPair[24]) for individually training random forest models. Stratified 50/50% train-test splitting with cross-validation (Table S5) revealed high prediction accuracy for all models. All three models predicted cinalukast as highly active (class 1) and agreed in the classification of compounds **4** and **4a-d** which were assigned to class 2 with high

confidence (Table 1). In light of the close structural similarity of **4** and **4a-d** to the known $CysLT_1R$ antagonist **1**, this ligand-based activity prediction seems reasonable.

Moreover, the predictions agreed with the limited data on the SAR of cinalukast (**1**) and derivatives as $CysLT_1R$ antagonists available in literature[25] which suggest importance of the 2,2-diethyl-4-oxobutanoic acid residue both in terms of chain length and ethyl substituents as well as of a small aliphatic ring as thiazole substituent for high potency on $CysLT_1R$. The latter is also reflected by SAR data for other $CysLT_1R$ antagonists such as zafirlukast[6,26,27] where small terminal aliphatic rings (cyclobutyl, cyclopentyl) were essential for antagonism while larger rings were markedly less active.

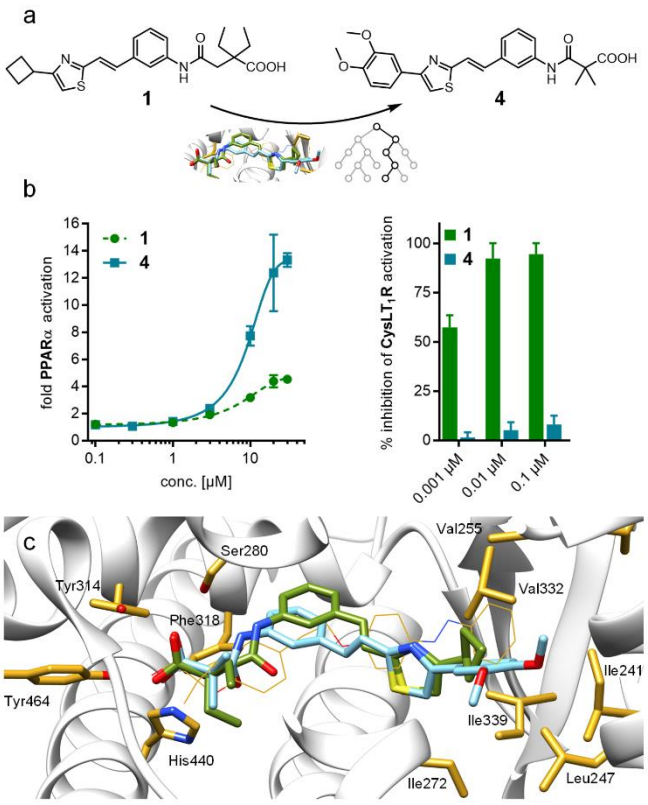

Figure 1. (a) Automated docking in the PPARα ligand binding site (PDB-ID: 4CI4[20]) and HYDE scoring combined with a random forest model trained on fingerprint representations of known $CysLT_1R$ antagonists successfully classified cinalukast analogue **4** for enhanced PPARα agonism and diminished $CysLT_1R$ antagonistic potency. (b) In vitro characterization of the computationally favored analogue **4** revealed enhanced PPARα activation efficacy and strongly reduced antagonism on $CysLT_1R$ (inhibition of $CysLT_1R$ activation by 0.1 nM leukotriene D4). Results are the mean ± S.E.M., n≥3 for PPARα, n=2 for $CysLT_1R$. (c) Predicted binding modes of **1** (green) and **4** (blue) in the PPARα ligand binding site (PDB-ID: 4CI4[20], co-crystallized ligand as yellow wire; docking was performed with FlexX and visualized with UCSF Chimera[28]). **1** and **4** form a very similar binding mode. The carboxylic acid residues of **1** and **4** participate in the canonical hydrogen bond network with Ser280, Tyr314, Tyr464 and His440 of the PPARα LBD. The styrylthiazole of **4** is slightly shifted towards the polar end of the binding site due to its shorter carboxylic acid side chain. The cyclobutyl (**1**) and dimethoxyphenyl (**4**) substituents occupy the lipophilic cavity at the end of the pocket, where the latter moiety seems to fill the available lipophilic space more favorably.

Cinalukast analogue **4** comprising a shortened 2,2-dimethyl-3-oxopropionic acid side chain and a bulky dimethoxyphenyl substituent on the thiazole was selected for synthesis (Scheme 1) and in vitro characterization based on its favorable activity prediction profile and building block availability. In vitro characterization of **4** revealed robust PPARα activation (13.7±0.1-fold) with an EC_{50} value of 8.1±0.1 μM and markedly reduced activity on $CysLT_1R$ compared to lead compound **1** (Figure 1b). Thus, the structural modifications caused a remarkable activity shift with enhanced PPARα activation efficacy (**4**: 13.7-fold vs. **1**: 5.3-fold) and strongly reduced antagonistic activity on $CysLT_1R$ (**4**: IC_{50} >> 100 nM vs. **1**: IC_{50} ~ 1 nM). Moreover, with an aqueous solubility of 21.7 mg/L (48 μM) and preferable lipophilicity (logP 1.6), **4** even exceeded the favorable properties of lead compound **1** (1.1 mg/L, 2.7 μM; logP 2.2) further confirming successful SOSA. Inspection of the predicted binding mode (Figure 1c) of **4** in the PPARα ligand binding site compared to **1** revealed only minor differences which agrees with the compounds' very similar HYDE scores. Participation in the canonical hydrogen bond network with Ser280, Tyr314, Tyr464 and His440 was observed for both compounds. Due to its shortened acidic chain, the styrylthiazole moiety of **4** was slightly shifted to this region of the binding site. As a consequence, the benzene ring was bound in closer proximity to Phe318. The large lipophilic cavity at the end of the PPARα ligand binding site formed by Ile241, Leu247, Leu254, Cys275 and Val332 accommodated the thiazole 4-substituents of both **1** and **4** but appeared more favorably occupied by the dimethoxyphenyl residue of **4**.

Conclusions

Combining virtual activity prediction and selective optimization of side-activities appears very promising for refining side-target activities of approved drugs towards bioactive new chemical entities with minimized experimental efforts. Since the basic concept of SOSA often demands that structural modifications are confined during optimization in order to conserve the favorable profile of the lead drug, focused virtual libraries of suitable analogues for optimization can be generated. We hypothesized that their computational prioritization is then capable of reducing time and cost intensive design-synthesize-test cycles and can speed up structural optimization for selective activity on the desired target.

Following this concept, we have employed the $CysLT_1R$ antagonist cinalukast (**1**) as lead for computer-assisted SOSA towards PPARα agonism. HYDE was chosen as computational scoring approach for PPARα activity as it was successfully applied to highly lipophilic binding sites as found in PPARs, previously, and yielded reliable results in a proof-of-concept evaluation. $CysLT_1R$ antagonism was computationally predicted using a random forest model as classifier between high and low $CysLT_1R$ antagonistic potency. From a virtual combinatorial library of close cinalukast analogues, **4** was computationally favored both in terms of high predicted affinity to PPARα and low estimated $CysLT_1R$ antagonism, and was consequently selected for synthesis and characterization. In vitro profiling of **4** confirmed the predicted activity shift towards higher activation efficacy on PPARα and markedly improved selectivity over $CysLT_1R$. Thus, our straightforward computational approach to analogue selection for SOSA successfully predicted the activity profile of **4**.

The strong activity shift achieved by the computationally selected cinalukast analogue **4** corroborates the potential of applying modern activity prediction techniques on structural compound

optimization in early drug discovery. It suggests that experimental efforts in (SOSA-based) optimization of drug molecules towards desired activity profiles can be markedly reduced by automated analogue design and scoring.

Acknowledgements

The authors thank Dr. Francesca Grisoni and Dr. Franca Klingler for scientific advice and technical support. The free use of the BioSolveIT chemoinformatics software suite as part of the scientific challenge is gratefully acknowledged. Molecular graphics and analyses performed with UCSF Chimera, developed by the Resource for Biocomputing, Visualization, and Informatics at the University of California, San Francisco, with support from NIH P41-GM103311.

Keywords: automation • peroxisome proliferator-activated receptor • nuclear receptor • virtual combinatorial library

Associated Content

Supporting Information available. The Supporting Information contains Supplementary Tables S1-S5, computational methods and model validation, synthetic procedures and analytical characterization of **2**-**4** and their precursors, data on evaluation of *E/Z*-isomerism, as well as methods for *in vitro* characterization.

Compound datasets used in this study and predicted binding poses for HYDE assessment are provided as sdf or csv files.

References:

[1] G. Schneider, *Nat. Rev. Drug Discov.* **2017**, *17*, 97–113.

[2] C. G. Wermuth, *J. Med. Chem.* **2004**, *47*, 1303–14.

[3] T. Langer, C. G. Wermuth, in *Polypharmacology Drug Discov.*, John Wiley & Sons, Inc., Hoboken, NJ, USA, **2012**, pp. 227–243.

[4] L. Michalik, J. Auwerx, J. P. Berger, V. K. Chatterjee, C. K. Glass, F. J. Gonzalez, P. A. Grimaldi, T. Kadowaki, M. A. Lazar, S. O'Rahilly, et al., *Pharmacol. Rev.* **2006**, *58*, 726–741.

[5] C. Lamers, M. Schubert-Zsilavecz, D. Merk, *Expert Opin. Ther. Pat.* **2012**, *22*, 803–841.

[6] E. Proschak, P. Heitel, L. Kalinowsky, D. Merk, *J. Med. Chem.* **2017**, *60*, 5235–5266.

[7] M. O'Donnell, *Ann. N. Y. Acad. Sci.* **1991**, *629*, 413–5.

[8] M. O'Donnell, H. J. Crowley, B. Yaremko, N. O'Neill, A. F. Welton, *J. Pharmacol. Exp. Ther.* **1991**, *259*, 751–8.

[9] J. Schmidt, M. Rotter, T. Weiser, S. Wittmann, L. Weizel, A. Kaiser, J. Heering, T. Goebel, C. Angioni, M. Wurglics, et al., *J. Med. Chem.* **2017**, *60*, 7703–7724.

[10] D. Flesch, S.-Y. Cheung, J. Schmidt, M. Gabler, P. Heitel, J. S. Kramer, A. Kaiser, M. Hartmann, M. Lindner, K. Lüddens-Dämgen, et al., *J. Med. Chem.* **2017**, *60*, 7199–7205.

[11] H. M. Sarau, R. S. Ames, J. Chambers, C. Ellis, N. Elshourbagy, J. J. Foley, D. B. Schmidt, R. M. Muccitelli, O. Jenkins, P. R. Murdock, et al., *Mol. Pharmacol.* **1999**, *56*, 657–63.

[12] N. Schneider, G. Lange, S. Hindle, R. Klein, M. Rarey, *J. Comput. Aided. Mol. Des.* **2013**, *27*, 15–29.

[13] H. A. Carlson, R. D. Smith, K. L. Damm-Ganamet, J. A. Stuckey, A. Ahmed, M. A. Convery, D. O. Somers, M. Kranz, P. A. Elkins, G. Cui, et al., *J. Chem. Inf. Model.* **2016**, *56*, 1063–1077.

[14] C. Ruggeri, N. Drinkwater, K. K. Sivaraman, R. S. Bamert, S. McGowan, A. Paiardini, *PLoS One* **2015**, *10*, e0138957.

[15] Z. Gaieb, S. Liu, S. Gathiaka, M. Chiu, H. Yang, C. Shao, V. A. Feher, W. P. Walters, B. Kuhn, M. G. Rudolph, et al., *J. Comput. Aided. Mol. Des.* **2018**, *32*, 1–20.

[16] P. da Silva Figueiredo Celestino Gomes, F. Da Silva, G. Bret, D. Rognan, *J. Comput. Aided. Mol. Des.* **2018**, *32*, 75–87.

[17] M. Su, Q. Yang, Y. Du, G. Feng, Z. Liu, Y. Li, R. Wang, *J. Chem. Inf. Model.* **2019**, *59*, 895–913.

[18] J. Weber, M. Rupp, E. Proschak, *Mol. Inform.* **2012**, *31*, 631–633.

[19] M. Rarey, B. Kramer, T. Lengauer, G. Klebe, *J. Mol. Biol.* **1996**, *261*, 470–89.

[20] J. C. dos Santos, A. Bernardes, L. Giampietro, A. Ammazzalorso, B. De Filippis, R. Amoroso, I. Polikarpov, *J. Struct. Biol.* **2015**, *191*, 332–340.

[21] A. P. Bento, A. Gaulton, A. Hersey, L. J. Bellis, J. Chambers, M. Davies, F. A. Krüger, Y. Light, L. Mak, S. McGlinchey, et al., *Nucleic Acids Res.* **2014**, *42*, D1083–D1090.

[22] J. L. Durant, B. A. Leland, D. R. Henry, J. G. Nourse, *J. Chem. Inf. Comput. Sci.* **2002**, *42*, 1273–1280.

[23] H. L. Morgan, *J. Chem. Doc.* **1965**, *5*, 107–113.

[24] R. E. Carhart, D. H. Smith, R. Venkataraghavan, *J. Chem. Inf. Model.* **1985**, *25*, 64–73.

[25] G. F. Field, J. R. Vermeulen, W. J. Zally, *Cycloalkylthiazole Derivatives*, **1990**, EP0355353A2.

[26] F. J. Brown, Y. K. Yee, L. A. Cronk, K. C. Hebbel, R. D. Krell, D. W. Snyder, *J. Med. Chem.* **1990**, *33*, 1771–1781.

[27] S. Schierle, C. Flauaus, P. Heitel, S. Willems, J. Schmidt, A. Kaiser, L. Weizel, T. Goebel, A. S. Kahnt, G. Geisslinger, et al., *J. Med. Chem.* **2018**, *61*, 5758–5764.

[28] E. F. Pettersen, T. D. Goddard, C. C. Huang, G. S. Couch, D. M. Greenblatt, E. C. Meng, T. E. Ferrin, *J. Comput. Chem.* **2004**, *25*, 1605–1612.

Entry for the Table of Contents

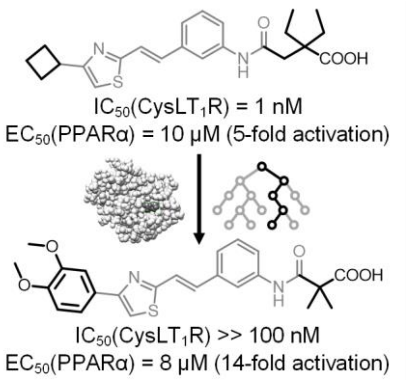

Selective optimization of side-activities (SOSA) aims to invert activity profiles of drug molecules. We have automated this approach using the $CysLT_1R$ antagonist cinalukast as lead which has a weak side-activity on PPARα. Automated analogue design and scoring produced a descendant of the drug that was experimentally confirmed as more active and markedly more selective towards the side-target corroborating the concept of computer-assisted SOSA.